Int. J. Environ. Sci. Technol. (2016) 13:2127–2134
DOI 10.1007/s13762-016-1049-5

ORIGINAL PAPER

Recovery of Zn from wastewater of zinc plating industry by precipitation of doped ZnO nanoparticles

M. John[1] · S. Heuss-Aßbichler[1] · A. Ullrich[2]

Received: 3 February 2016 / Revised: 9 May 2016 / Accepted: 27 June 2016 / Published online: 12 July 2016

Abstract In this study, a facile precipitation process to treat wastewater from zinc plating industry is presented. Water purification rates of Zn range between 96.40 % and 99.99 % depending on the reaction conditions. Optimal results are gained at a low pH value of 9, low temperature of 40 °C and a fast alkalization using NaOH solution containing 16 % pure NaOH. Traces of Ni, Fe, Zn, Cu and Cr present in the wastewater were almost completely removed. The precipitates were analysed by X-ray diffraction, infrared and Raman spectroscopy, electron microscopy and magnetic measurements. They consist of doped ZnO as a main phase. Although ZnO exclusively crystallizes in nanoparticle size, the morphology is directly influenced by the experimental parameters. Additionally, very small amounts of $ZnCO_3$ and $Zn(OH)_2$ were detected. Magnetic investigations indicate the incorporation of Ni and Fe into the ZnO lattice. The measured saturation magnetization is ~0.01 emu/g and the Curie temperature is ~75 °C.

Keywords Avoidance of hydroxides · Nanosized precipitates · Wastewater treatment · Zincite

Introduction

Zinc represents an important raw material for diverse industrial applications. In consequence in various industrial branches, as electroplating companies and metal finishing industries wastewater loaded with zinc and other heavy metals are produced. Though there are various techniques as chemical precipitation, adsorption, ion exchange or membrane filtration to treat wastewater (Fu and Wang 2011), especially in developing countries heavy metal containing wastewater is directly or indirectly discharged into the environment. For this reason, heavy metal pollution has become one of the most serious environmental problems today. The commonly used method to treat this wastewater is the precipitation of heavy metals as hydroxides because it is simple and low cost (Huisman et al. 2006). However, this treatment causes a very high volume of sludge finally leading to disposal problems (Kongsricharoern and Polprasert 1995). Based on their high water and low heavy metal content, only small fractions of the sludge are recycled. Another technique to remove low concentrations of bivalent cations from laboratory wastewater is to incorporate them into the ferrite structure (Katsura et al. 1977; Okuda et al. 1975; Barrado et al. 1998). However, the so-called ferrite process does not necessarily lead to a monophasic residue which is low in volume (Pritosiwi 2012; Heuss-Aßbichler et al. 2014; John and Heuss-Aßbichler 2015).

On the one hand, zinc is an essential element for good health, but at high concentrations it can be harmful (Sandstead 1995). On the other hand, ZnO nanoparticles are in focus of both industry and research due to many possible applications including UV lasers (Chu et al. 2011), solar cells (Matsubara et al. 2003; Sudhagar et al. 2011), photodetectors (Hsu et al. 2005), gas sensors (Xu et al.

✉ M. John
melanie.john@min.uni-muenchen.de

[1] Department of Earth and Environmental Sciences, Ludwig-Maximilians-Universität München, Theresienstr. 41, 80333 Munich, Germany

[2] Experimental Physics II, University of Augsburg, Universitätsstr. 1, 86159 Augsburg, Germany

2008; Wang et al. 2012) and piezoelectric devices (Wang et al. 2010) depending on its morphology and doping. Hence, there are various techniques to synthesize ZnO, e.g. solid-state reactions, hydrothermal procedures (Chen et al. 2000; Zhang et al. 2012), hydrolysis (Jezequel et al. 1995), solution routs (Zhang et al. 2002; Desai and Sartale 2015) and vapour phase synthesis (Zhang et al. 2012).

In focus of our study is the development of a procedure (1) to purify heavy metal, especially zinc-loaded wastewater from zinc plating industry by a facile, single-step precipitation process, and (2) to gain nanocrystalline ZnO free of hydroxides.

Materials and methods

Materials: wastewater from zinc plating industry

The experiments were performed using wastewater from zinc plating industry containing almost 1.4 g/l zinc and traces of copper, nickel, chromium and iron of <2 mg/l. Table 1 summarizes the heavy metal concentrations (>0.05 mg/l) measured in the wastewater by ICP-OES.

Experimental set-up

First, 150 ml of wastewater from zinc plating industry was heated up to the reaction temperature (40–90 °C). As a next step NaOH (solution with 4–16 % pure NaOH, VWR analytical grade) was added until the reaction pH (pH 9–11) was reached. Afterwards the pH was maintained at reaction pH for 3 min.

During these two steps, the solution was continuously stirred and kept at reaction temperature. Afterwards a 50-ml aliquot was taken representing freshly precipitated particles (=fresh sample). The remaining solution was filled in two conventional laboratory bottles. The bottles were sealed and stored either at elevated temperature (=et, equal the particular reaction temperature) or at room temperature (=rt) for 24 h.

Afterwards the precipitates were filtered, washed 3 times with water (5 µS/cm) and dried at room temperature for 12 h. For pH measurements and adjustments, a Titrator TL 7000 (SI Analytics) was used.

Table 1 Heavy metal concentration (>0.05 mg/l) in wastewater from zinc plating industry

Concentration (mg/l)				
Zn	Cu	Ni	Cr	Fe
1392.12	0.74	1.37	0.28	1.91

Methods

Inductively coupled plasma optical emission spectrometry (ICP-OES)

ICP-OES measurements were performed on an ICP JY 70+ from Horiba Jobin–Yvon GmbH [Department for Earth and Environmental Sciences (DEES), Ludwig-Maximilians Universität (LMU) München] to analyse the metal concentration of the industrial wastewater before and after the treatment. The detailed measurement conditions and the SD are summarized in Table 2.

X-ray powder diffraction (XRD)

Phase identification was performed by X-ray powder diffraction on a GE SEIFERT XRD 3003 TT (DEES–LMU München). All measurements were carried out using $CuK_{\alpha 1}$ radiation on zero-background quartz holders. Each pattern was measured for 3 times and added up to achieve a better signal-to-noise ratio. The sample holder was rotated during the measurement for getting a better counting statistics. After the diffraction pattern was corrected for baseline, phase identification was carried out with the help of the software FindIt and based on reference inorganic crystal structure database (ICSD).

Fourier transform infrared spectroscopy (FTIR)

FTIR spectra were used to identify low crystalline phases. All measurements were performed on a FTIR spectrometer EQUINOX55 from Bruker (DEES–LMU München). The data were corrected for atmospheric influences and baseline. Typically, the spectra were fitted with the software PeakFit. The identification of peaks was done with the help of literature references from RRUFF database (Lafuente et al. 2015).

Table 2 Element-specific parameters for performed ICP-OES measurements

Element	Wavelength (nm)	Detection limit (mg/l)	SD (%)
Cu	324.754	0.0054	0.2
	213.598	0.0120	0.2
Cr	284.325	0.0086	0.9
Fe	238.204	0.0046	0.8
	259.940	0.0062	1.1
Ni	231.604	0.0140	0.4
	234.554	0.0310	0.5
Zn	213.856	0.0018	0.5
	330.259	0.2300	0.4

Raman spectroscopy

Raman measurements were performed on a Horiba XploRA system mounted on an Olympus BX51 microscope (Mineralogical State Collection Munich) using a 532.14 laser. The phases were identified by comparison of the recorded spectra with RRUFF database (Lafuente et al. 2015).

Scanning electron microscopy (SEM)

The SEM investigations were carried out with the NanoSAM Lab from Scienta Omicron, using a UHV Gemini column with an ultimate resolution of <3 nm (Universität Augsburg). All pictures were taken at 10 kV beam energy, a beam current of 100 pA and a working distance of 5 mm with the inlens detector.

Transmission electron microscopy (TEM) and EDS analyses

TEM measurements were performed using a JEOL JEM-2100F transmission electron microscope equipped with both a Gatan imaging filter for energy-filtered microscopy and an EDAX EDS detector for recording the chemical composition. Particle size and shape investigations were carried out in the imaging mode, supplemented by electron diffraction for structural analysis.

Variable field translation balance (VFTB)

Magnetic responses to an applied magnetic field between −9000 and 9000 Oe were carried out at room temperature on a VFTB from Petersen Instruments (DEES–LMU München).

Results and discussion

In this study, we present six experimental series performed at pH values of 9 and 11, temperatures at 40, 70 and 90 °C and varying ageing conditions to demonstrate the influence of experimental parameters on (1) quality of the wastewater purification and (2) the precipitates.

Samples are named according to the following convention: "reaction temperature"_"pH-value"_"concentration of added Na(OH) solution". "_fresh" stands for a sample that was not aged. The supplement of "_et" means ageing at elevated temperature (=et) for 24 h, and "_rt" stands for ageing at room temperature (=rt) for 24 h.

Wastewater purification

Table 3 summarizes the concentration of heavy metals in the wastewater after the precipitation process. Optimal conditions for zinc purification rates of $\geq$99.87 % were achieved at pH 9 and 40 °C (sample series 40_9_4 and

Table 3 Metal content of wastewater measured after the precipitation process and the corresponding purification rate (=PR) for zinc. The supplement "_f" stands for fresh sample without ageing

Sample	pH	Reaction temperature	Ageing temperature	PR (Zn) (%)	Concentration (mg/l)	
					Zn	Cu, Ni, Cr, Fe
40_9_4_f	9	40	No	99.92	1.06	<0.01
40_9_4_et	9	40	40	99.96	0.61	
40_9_4_rt	9	40	20	99.87	1.79	
40_9_16_f	9	40	No	99.99	0.11	
40_9_16_et	9	40	40	99.99	0.08	
40_9_16_rt	9	40	20	99.93	1.03	
40_11_4_f	11	40	No	99.77	3.24	
40_11_4_et	11	40	40	99.77	3.19	
40_11_4_rt	11	40	20	99.73	3.72	
40_11_16_f	11	40	No	99.83	2.32	
40_11_16_et	11	40	40	99.84	2.28	
40_11_16_rt	11	40	20	99.78	3.11	
70_11_16_f	11	70	No	99.28	10.01	
70_11_16_et	11	70	70	99.23	10.78	
70_11_16_rt	11	70	20	99.32	9.53	
90_11_16_f	11	90	No	96.76	45.09	
90_11_16_et	11	90	90	96.40	50.16	
90_11_16_rt	11	90	20	97.59	33.53	

40_9_16). Purification rates of experiments after using solutions with 16 % pure NaOH are higher than the corresponding experiments with 4 % NaOH solutions. The best result with a purification rate of 99.99 % achieved the samples 40_9_16_f and 40_9_16_et. After treatment, the zinc concentration in these samples was $\leq$0.11 mg/l. This value is far below the critical value of 3 mg/l defined by the World Health Organization (WHO).

At higher pH value of 11, the purification rate was between 99.77 % and 99.84 %. By increasing the reaction temperatures to 70 and 90 °C, the zinc purification rates of the wastewater dropped below 99.32 %. The worst purification rates <97.6 % are attained for the sample series 90_11_16 with zinc concentrations up to 50.16 mg/l in the solution.

Ageing conditions also influence the quality of the wastewater. Treating the samples at 40 °C and ageing at elevated temperature improved the purification rate compared to the fresh samples or samples aged at room temperature. In contrast at higher reaction temperatures, the purification rates were better if the samples aged at room temperature (sample series 70_11_16 and 90_11_16, see Table 3).

It is noteworthy that independently of the reaction conditions Cu, Ni, Cr and Fe present in the initial wastewater in low amounts are removed by the precipitation process. Thereafter the remaining concentrations were exclusively <0.01 mg/l.

Characterization of nanocrystalline precipitates

In all cases the products are nanocrystals. Following we present the results obtained from sample series with a purifications rate better than 99.2 % performed at 40 and 70 °C.

Phase analyses: XRD, FTIR and Raman

All precipitation products consist of ZnO as the only crystalline phase. X-ray patterns of fresh precipitates from sample series 40_9_4&_16, 40_11_4&_16 and 70_11_16 presented in Fig. 1 clearly show differing intensities of the (100), (002) and (101) reflexes depending on the experimental conditions. The peak position corresponds exactly to the ZnO position. Obviously, the amount of foreign ions is too small to have an effect.

At pH 9 and 40 °C, the (100), (002) and (101) reflexes of the sample series 40_9_4&_16 show ascending intensities. At a higher pH value of 11 (sample series 40_11_4&_16), the intensity of the (002) and (101) reflexes are almost equal. By increasing the reaction temperature from 40 to 70 °C (sample 70_11_16), the intensity of the (002) reflex clearly decreases. The absolute intensities of the observed reflexes are highest for samples 40_9_16 and 70_11_16 indicating good crystallinity of ZnO. All other sample series precipitated either at 40 °C and pH 11 or using low-concentrated Na(OH) solution [containing 4 % pure Na(OH)] show broader peaks with lower intensities.

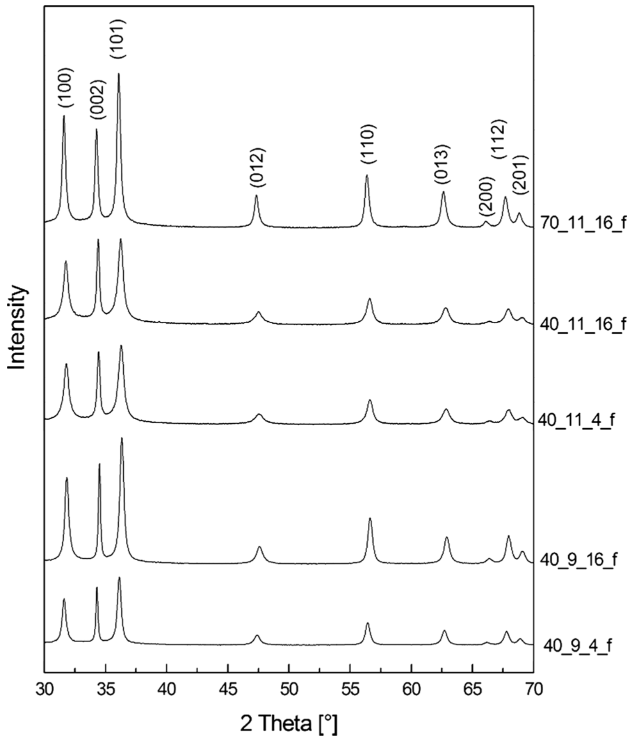

Fig. 1 X-ray pattern of fresh precipitates obtained at pH 9 and 11 at 40 and 70 °C using different concentrated (4 or 16 %) Na(OH) solutions

Different intensities of the reflexes are obviously due to variable morphology of the ZnO particles. This assumption is in line with previous works (Wu et al. 2007).

The FTIR spectra of the fresh samples are shown in Fig. 2. In accordance with the X-ray data, the precipitates consist mainly of ZnO. Sample 40_9_4 shows an intensive absorbance band at 417 cm^{-1} attributed to the characteristic vibrational mode of Zn–O bonding (Nagaraju et al. 2010) and a much weaker band at 580 cm^{-1}. Additional very weak bands at 713, 872, 1135, 1400 and 1498 cm^{-1} correspond to a very small amount of low crystalline ZnCO$_3$ (smithsonite), and very weak bands at 445, 470, 1626, 3200 and 3400 cm^{-1} are assigned to traces of Zn(OH)$_2$. Traces of ZnCO$_3$ and Zn(OH)$_2$ are probably adsorbed on the surface of the crystalline ZnO particles which clearly represent the main phase in all precipitates.

By using a NaOH solution containing 16 % pure NaOH (sample 4_9_16) instead of a low-concentrated one (sample 40_9_4), the amount of ZnCO$_3$ and Zn(OH)$_2$ markedly increases.

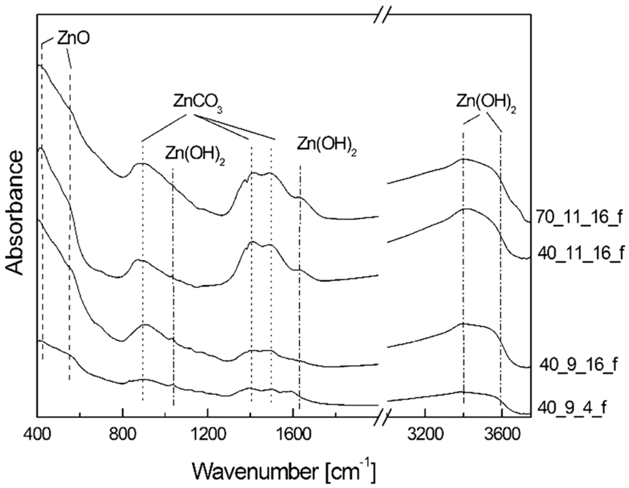

Fig. 2 FTIR spectra of fresh precipitates obtained at pH 9 and 11 at 40 and 70 °C using different concentrated (4 or 16 %) NaOH solutions. All spectra show the presence of ZnO and small amounts of $ZnCO_3$ and $Zn(OH)_2$

The absorbance bands at 1400 and 1498 cm^{-1} are stronger in the experiments performed at higher pH of 11 and higher temperature of 70 °C (sample 4_11_16 and 70_1_16) indicating a higher content of $ZnCO_3$ in these samples. By varying the ageing conditions, no trend can be observed.

The Raman spectrum of sample 40_11_16_f in Fig. 3 exhibits two main peaks at 213 and 1142 cm^{-1}. The observed bands do not fit in with the characteristic Raman peaks of ZnO nanoparticles at 332, 383 and 437 cm^{-1}. However, there are a few studies reporting partially strongly deviating or additional Raman modes for doped ZnO: Cong et al. (2006) published two additional Raman modes at 813 and 891 cm^{-1} for ZnO nanoparticles doped with nickel. An additional mode at 720 cm^{-1} is found when Fe doped (Bundesmann et al. 2003). $ZnCO_3$ typically shows Raman modes at 198, 300 and 1095 cm^{-1}. They correspond very well with our spectrum. Based on our preparation method leading to distinct orientation, only specific bands of the particles are detectable. The distinct shift of the bands is obviously effected by the incorporation of the foreign elements Cu, Cr, Fe and Ni.

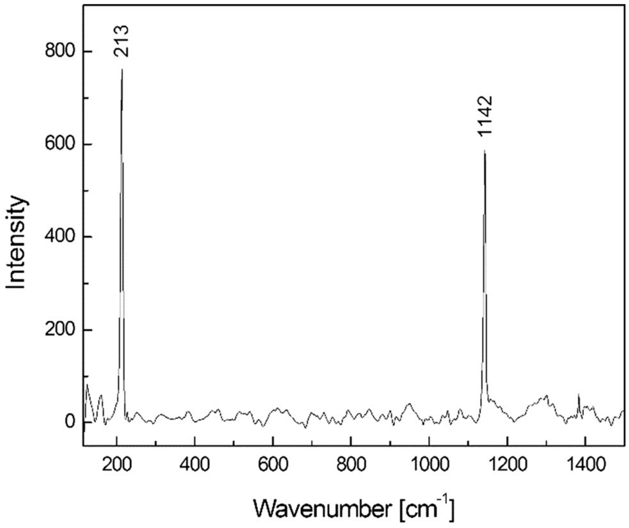

Fig. 3 Raman spectrum of sample 40_11_16_f showing two main Raman modes at 213 and 1142 cm^{-1}

Morphology and chemistry: SEM and TEM

Figure 4 shows SEM images of the precipitates of the experimental series 40_9_4&_16, 40_11_4&16 and 70_11_16. The size of the particle is obviously controlled by pH and temperature.

Precipitates prepared at pH 9 (Fig. 4a–e) consist of elongated ZnO nanoprisms with an average size of 200–100 nm. Particles of the fresh sample series 40_9_4 show well-defined edges and rough surfaces (see Fig. 4a, b). In contrast the particles obtained after 1 day at 40 °C ageing temperature (40_9_4_et, see Fig. 4c, d) or precipitated by the addition of higher-concentrated NaOH (sample series 40_9_16) are characterized by smooth surfaces and diffuse edges (see Fig. 4e). At a reaction pH of 11 (sample series 40_11_4 and 40_11_16), the morphology of the particles is more rounded with an average size of 100–150 nm (Fig. 4f, g). At a higher reaction temperature (sample series 70_11_16), ZnO crystallizes as rounded nanoflakes with a diameter of 25–50 nm (Fig. 4h).

TEM images of sample 40_9_4_f and 70_11_16 verifying the morphologies are observed in the SEM images (Fig. 5a, e). The 100- to 200-nm large ZnO particles are composed of many small crystallites. The dominant crystallite size is within the range of 5–10 nm as illustrated in Fig. 5b, c, h. All ZnO particles are highly crystalline, and the measured lattice spacing in HRTEM images perfectly matches to ZnO (Fig. 5d, g). No other phases except ZnO were detected. The diffuse rim observed for some particles (Fig. 5d, f) may be the effect of absorbance or accretion of very small amounts of $Zn(OH)_2$ or $Zn(CO)_3$ as already observed by FTIR and Raman measurements.

Furthermore, EDS measurements on 50 randomly chosen particles were performed. All measured data points indicate an homogeneous and consistent ratio of 80 wt% Zn/20 wt% O. This corresponds to an atomic ratio of almost 1/1 in the precipitated particles. Additionally, very small signals of Ni, Fe and Cr (in descending intensity) are detectable. However, the amount of these elements is too low to get a quantitative result.

Magnetic properties of nanocrystalline precipitates

To verify the incorporation of magnetic ions into the ZnO structure during the precipitation process, magnetic

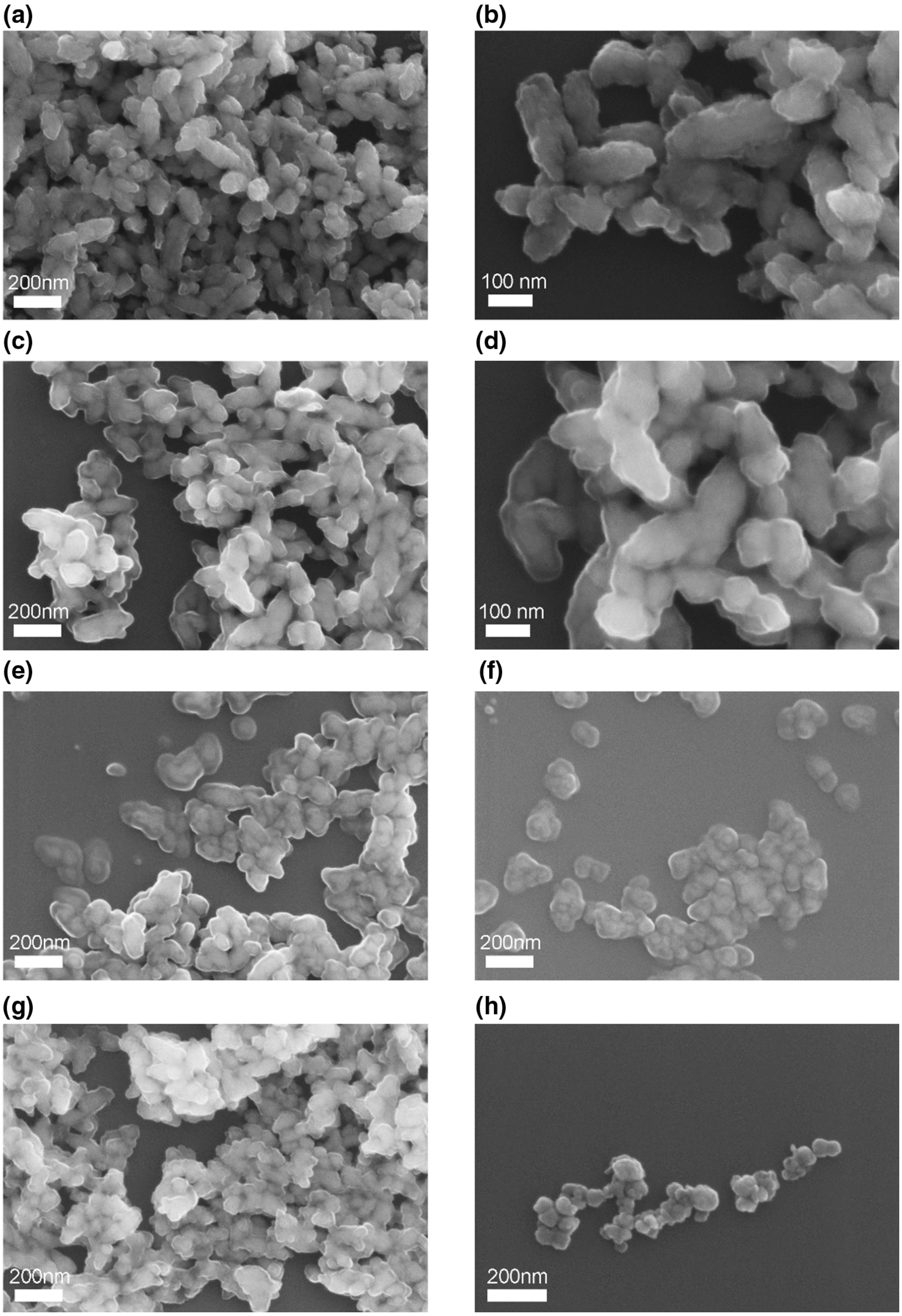

Fig. 4 SEM images of the precipitates of **a**, **b** sample 40_9_4_f, **c**, **d** sample 40_9_4_et, **e** sample 40_9_16, **f** sample 40_11_4, **g** sample 40_11_16 and **h** sample 70_11_16

measurements at room temperature were carried out. While pure ZnO is diamagnetic doping with nickel (Cong et al. 2006), iron and copper (Han et al. 2002; Karmakar et al. 2007) leads to ferromagnetic properties at room temperature.

Figure 6 presents the magnetic hysteresis (M–H) loop of sample 70_11_16_f showing clearly an s-shape around the origin indicating a ferromagnetic contribution. No remanent magnetization is detected. The measured saturation magnetization is ~0.01 emu/g and the Curie temperature ~75 °C. These results are generally in line with the observations of Wang et al. (2007) for nickel-doped ZnO.

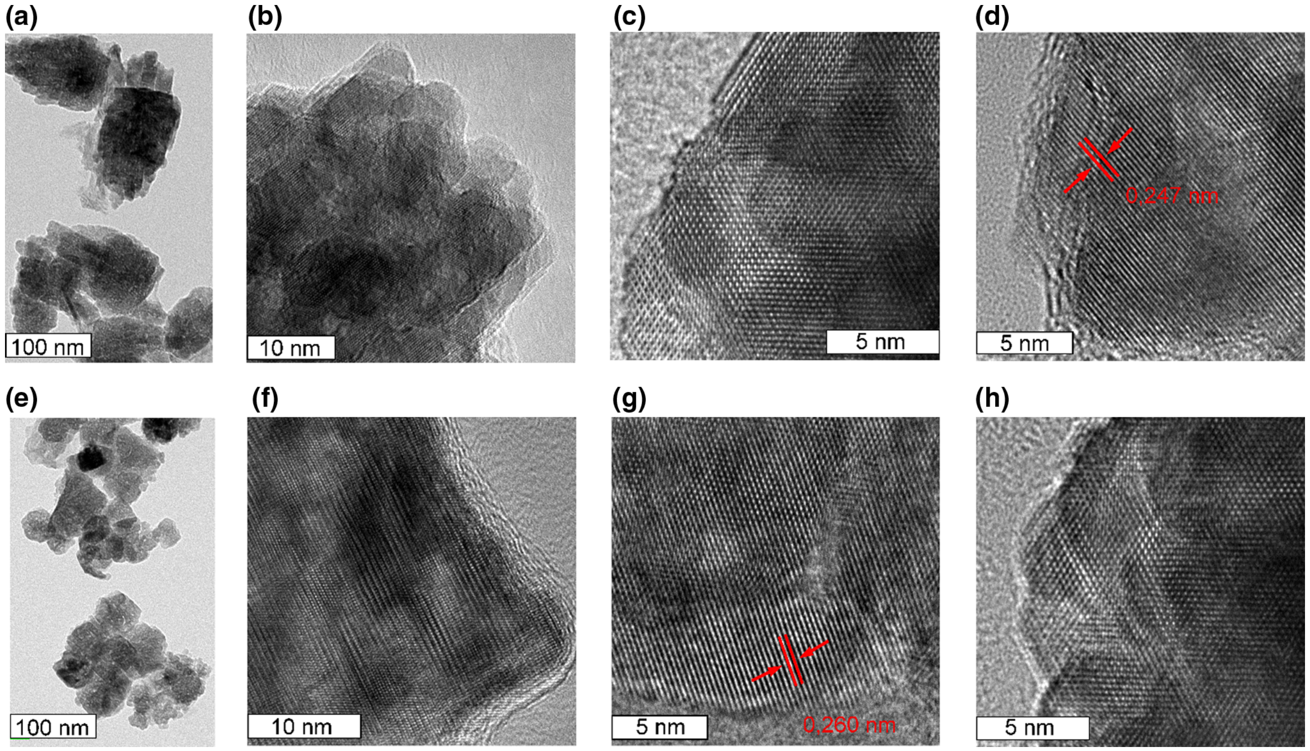

Fig. 5 TEM images of **a**–**d** sample 40_9_4_f and **d**–**h** sample 70_11_16_f

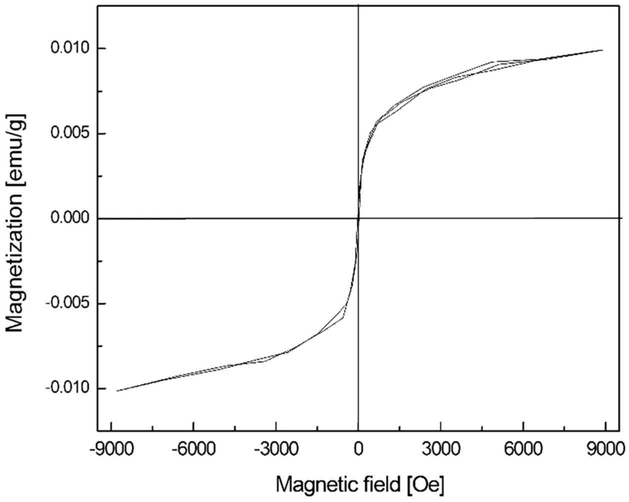

Fig. 6 Hysteresis loop at room temperature of sample 70_11_16_f showing an s-shape around the origin. This indicates an incorporation of foreign ions as Ni, Cu or Fe into the ZnO structure

Conclusion

The commonly used neutralization treatment methods produce voluminous residues containing mainly hydroxides. Herein, we present a facile technique to treat wastewater from zinc plating industry by the precipitation of heavy metal-doped ZnO nanoparticles. With our method we can successfully recover zinc. The residues consist of nanocrystalline-doped ZnO particles showing controllable morphology. The amount of coprecipitated phases is below the detection limit of X-ray diffraction. The main advantages of this method are water purification rates of 99.99 %. Optimal purification conditions are achieved at pH 9, 40 °C and for an alkalization with NaOH solution containing 16 % pure NaOH. In comparison the residues obtained herein are highly enriched in Zn and almost hydroxide free. By doping they can be attractive for industrial use. These improvements facilitate an economic and efficient recycling procedure.

Acknowledgments The authors thank Alexander Reul for his assistance in the lap and for performing the Raman measurement. Furthermore, the authors wish to thank Nikolai Petersen for his helpful advices regarding magnetic measurements and the corresponding data interpretation. The Mineralogical State Collection Munich is acknowledged for providing the Raman instrument. This study was supported by the Bavarian State Ministry of the Environment and Consumer Protection (StMUV) within the frame of ForCycle (#BAFO1SoFo-65214).

References

Barrado E, Prieto F, Vega M, Fernández-Polanco F (1998) Optimization of the operational variables of a medium-scale reactor for metal-containing wastewater purification by ferrite formation. Water Res 32(10):3055–3061

Bundesmann C, Ashkenov N, Schubert M, Spemann D, Butz T, Kaidashev EM, Grundmann M (2003) Raman scattering in ZnO thin films doped with Fe, Sb, Al, Ga, and Li. Appl Phys Lett 83:1974

Chen M, Wang X, Yu YH, Pei ZL, Bai XD, Sun C, Wen LS (2000) X-ray photoelectron spectroscopy and auger electron spectroscopy studies of Al-doped ZnO films. Appl Surf Sci 158(1):134–140

Chu S, Wang G, Zhou W, Lin Y, Chernyak L, Zhao J, Liu J (2011) Electrically pumped waveguide lasing from ZnO nanowires. Nat Nanotechnol 6(8):506–510

Cong CJ, Hong JH, Liu QY, Liao L, Zhang KL (2006) Synthesis, structure and ferromagnetic properties of Ni-doped ZnO nanoparticles. Solid State Commun 138(10):511–515

Desai MA, Sartale SD (2015) Facile soft solution route to engineer hierarchical morphologies of ZnO nanostructures. Cryst Growth Des 15(10):4813–4820

Fu F, Wang Q (2011) Removal of heavy metal ions from wastewaters: a review. J Environ Manag 92(3):407–418

Han SJ, Song JW, Yang CH, Park SH, Park JH, Jeong YH (2002) A key to room-temperature ferromagnetism in Fe-doped ZnO:Cu. http://arxiv.org/abs/0208399

Heuss-Aßbichler S, Klapper D, John M (2014) Mineralogical investigations of precipitates obtained by treatment of Cu-rich wastewater by ferrite process. Interfaces of Water and Environmental Science (IAP), Leeuwarden

Hsu CL, Chang SJ, Lin YR, Li PC, Lin TS, Tsai SY, Chen IC (2005) Ultraviolet photodetectors with low temperature synthesized vertical ZnO nanowires. Chem Phys Lett 416(1):75–78

Huisman JL, Schouten G, Schultz C (2006) Biologically produced sulphide for purification of process streams, effluent treatment and recovery of metals in the metal and mining industry. Hydrometallurgy 83(1):106–113

Jezequel D, Guenot J, Jouini N, Fievet, F (1995) Submicrometer zinc oxide particles: elaboration in polyol medium and morphological characteristics. J Mater Res 10(01):77–83

John M, Heuss-Aßbichler S (2015) Recovery of heavy metals by ferrite process: new results. In: Goldschmidt conference, Prague, Czech Republic

Karmakar D, Mandal SK, Kadam RM, Paulose PL, Rajarajan AK, Nath TK, Das GP (2007) Ferromagnetism in Fe-doped ZnO nanocrystals: experiment and theory. Phys Rev B 75(14):144404

Katsura T, Tamaura Y, Terada H (1977) ‘Ferrite process’ treatment of the wastewater from laboratories. Ind Water Jpn 223

Kongsricharoern N, Polprasert C (1995) Electrochemical precipitation of chromium (Cr^{6+}) from an electroplating wastewater. Water Sci Technol 31(9):109–117

Lafuente B, Downs RT, Yang H, Stone N (2015) The power of databases: the RRUFF project. In: Armbruster T, Danisi RM (eds) Highlights in mineralogical crystallography. W. De Gruyter, Berlin, pp 1–30

Matsubara K, Fons P, Iwata K, Yamada A, Sakurai K, Tampo H, Niki S (2003) ZnO transparent conducting films deposited by pulsed laser deposition for solar cell applications. Thin Solid Films 431:369–372

Nagaraju G, Ashoka S, Chithaiah P, Tharamani CN, Chandrappa GT (2010) Surfactant free hydrothermally derived ZnO nanowires, nanorods, microrods and their characterization. Mater Sci Semicond Process 13(1):21–28

Okuda T, Sugano I, Tsuji T (1975) Removal of heavy metals from waste-waters by ferrite co-precipitation. Filtr Sep 12(5):472–475

Pritosiwi G (2012). Removal of metal ions from synthetic und galvanic wastewater by their incorporation into ferrites. Dissertation, Technische Universität Hamburg-Harburg, Hamburg-Harburg Universitätsbibliothek

Sandstead HH (1995) Requirements and toxicity of essential trace elements, illustrated by zinc and copper. Am J Clin Nutr 61(3):621S

Sudhagar P, Kumar RS, Jung JH, Cho W, Sathyamoorthy R, Won J, Kang YS (2011) Facile synthesis of highly branched jacks-like ZnO nanorods and their applications in dye-sensitized solar cells. Mater Res Bull 46(9):1473–1479

Wang H, Chen Y, Wang HB, Zhang C, Yang FJ, Duan JX, Li Q (2007) High resolution transmission electron microscopy and Raman scattering studies of room temperature ferromagnetic Ni-doped ZnO nanocrystals. Appl Phys Lett 90(5):052505

Wang ZL, Yang R, Zhou J, Qin Y, Xu C, Hu Y, Xu S (2010) Lateral nanowire/nanobelt based nanogenerators, piezotronics and piezo-phototronics. Mater Sci Eng R Rep 70(3):320–329

Wang L, Kang Y, Liu X, Zhang S, Huang W, Wang S (2012) ZnO nanorod gas sensor for ethanol detection. Sens Actuators B Chem 162(1):237–243

Wu C, Qiao X, Chen J, Wang H (2007) Controllable ZnO morphology via simple template-free solution route. Mater Chem Phys 102(1):7–12

Xu J, Han J, Zhang Y, Sun YA, Xie B (2008) Studies on alcohol sensing mechanism of ZnO based gas sensors. Sens Actuators B Chem 132(1):334–339

Zhang J, Sun L, Yin J, Su H, Liao C, Yan C (2002) Control of ZnO morphology via a simple solution route. Chem Mater 14(10), 4172–4177

Zhang Y, Ram MK, Stefanakos EK, Goswami DY (2012) Synthesis, characterization, and applications of ZnO nanowires. J Nanomater 2012:20